Title
Optimal maintenance decisions for deteriorating quoin blocks in miter gates subject to uncertainty in the condition rating protocol

Authors
Vega, Manuel A
Hu, Zhen
Todd, Michael D

Publication Date
2020-12-01

DOI
10.1016/j.ress.2020.107147

Peer reviewed

Revision #2 to Reliability Engineering & System Safety

Optimal Maintenance Decisions for Deteriorating Quoin Blocks in Miter Gates Subject to Uncertainty in the Condition Rating Protocol

Manuel A. Vega[a], Zhen Hu[b], and Michael. D. Todd[a]*

[a] *Department of Structural Engineering,*
University of California San Diego,
9500 Gilman Dr., La Jolla, California, USA 92093-0085

[b] *Department of Industrial and Manufacturing Systems Engineering,*
University of Michigan-Dearborn,
4901 Evergreen Rd., Dearborn, Michigan, USA 48187
*Email: mdtodd@eng.ucsd.edu**

Abstract

Condition assessments and rating systems are frequently used by field engineers to assess inland navigation assets and components. The goal of these assessments is to initiate effective risk-informed budget plans for maintenance and repair/replace. Ideally, a degradation model of every component failure mode in the gate would facilitate maintenance decision-making. However, sometimes there is no clear physical understanding how a damage progresses in time; for example, it isn't clear how the bearing gaps change in time in the quoin blocks of a miter gate. Therefore, this is one motivation for the framework proposed in this paper, which integrates Structural Health Monitoring with a Markov transition matrix built from historical condition assessment. To show the applicability of this framework, two examples are presented of how to find the optimal time to plan for maintenance of components in miter gates i) static maintenance planning based on operational condition assessment (OCA) ratings only and ii) dynamic maintenance planning based on integration of damage diagnostics based on monitoring data and failure prognosis based on OCA ratings. In addition, this paper presents a new Bayesian approach to estimate the ratio of errors in the OCA ratings, which allows for improved accuracy in OCA rating-based prognosis.

Keywords: Miter gates; Uncertainty quantification; Weibull analysis, Surrogate model, Damage estimation, Bayesian, Remaining useful life, Markov process.

1. Introduction

The U.S. Army Corps of Engineers (USACE) maintains and operates 236 locks at 191 sites in the United States [1]. More than half of these structural assets have surpassed their 50-year economic design life [2]. For the USACE portfolio, a maintenance planning framework is needed for the navigation structures that are under the SMART Gate program [3], which consists of several lock sites including Dalles Navigation Lock, Lock 27, Greenup Lock (used in this work), and Meldahl Lock on the Mississippi River [4]. In this work, the component of interest is the bearing gap in the quoin blocks. The deterioration of the quoin blocks is broadly manifested as a small gap because of the loss of contact between the quoin block attached to the gate and the wall that supports the gate laterally. The formation of this gap can be detected using sensor data or from features derived from this data [5,6]. It is important to optimize the maintenance of quoin block components because they directly control the lateral boundary conditions, which affect the stress profile in horizontally-framed miter gates, where over-stresses exceeding a certain threshold can lead to structural failure. Currently, contact blocks are effectively a continuous single piece of steel, which during maintenance requires the entire piece to be replaced even if only part is damaged [7]. However, replacement cost is relatively low compared to the downtime cost during maintenance or when failure occurs. Therefore, it is necessary to optimize the maintenance considering not only repair/replacement costs but also the impact (consequence) costs when a miter gate is not operational.

Maintenance planning has been extensively studied for various engineering systems in the past decades. Current approaches can be roughly classified into two categories, namely time-based maintenance (TBM) and condition-based maintenance (CBM). TBM (also known as periodic maintenance) assumes that the estimated failure behavior is statistically or experientially known [8]. Statistical modelling such as Weibull analysis

[9] is widely used in TBM to identify failure characteristics of a component or system. The goal of TBM models is to find the optimal policy that minimizes a cost function. TBM approaches have been developed for both repairable or nonrepairable systems [10], and the complexity of the TBM approach correlates to the complexity of the structural system. Applications for single-component or multi-component systems are found in [11,12] and [13,14], respectively. A more extensive review of TBM applications can be found here [15]. In this work, a single component system TBM model is first considered and later compared with a CBM model.

CBM has gained increasing attention recently as a preferred approach to TBM. CBM combines data-driven reliability models and information from a condition monitoring process (e.g. continuous monitoring, periodic inspection, or non-periodic inspection). Based on the underlying degradation process, CBM models can be categorized into two subgroups: (1) models that assume discrete-state deterioration and (2) models that assume continuous state deterioration. An extensive list of CBM applications may be found in [16–19], primarily used for mechanical, aerospace, or manufacturing systems. For large civil engineering infrastructure, most of the applications have been applied specifically to bridge engineering [20–22]. In CBM, maintenance schedules are predicted based on methods integrating current state diagnostics and future state prognosis. These methods may be classified into physics-based (e.g., a finite element (FE) model) [23–25], data-driven (e.g., a Marko transition matrix or other probabilistic method) [26–29], and hybrid approaches [30,31]. A hybrid approach that combines physics-based knowledge with in-situ data to improve the CBM predictive capabilities is the focus of this paper. For the case of the miter gate (and many other structural applications), an FE model to predict the miter gate response for diagnostics is employed, due to the lack of field data. In order to use a physics-based approach for prognostics, a degradation state equation would be needed. The degradation of some critical components of the miter gate, however, is not fully well understood. A random-walk state equation could be assumed; as is shown in this paper, a random-walk state equation will lead to large errors, even though it might be good enough for damage diagnostics. This work proposes a new hybrid approach to overcome this challenge by integrating physics-based structural health monitoring (SHM) with a statistically-based state transition matrix, which is obtained from operational condition assessment (OCA) data. The OCA rating is an assessment obtained from an inspection process, which uses existing data from periodic and non-periodic inspections, including corrosion tests and dive reports. The objective of the OCA process is to obtain global consistent operational condition data to identify the current condition states of the USACE infrastructure [32]. According to the literature, hybrid approaches have not been studied as extensively as noted in [33] and even less for large civil infrastructure systems or miter gates. While the focus in this paper will be on horizontally-framed miter gates, the framework is applicable to other structures that have both online health monitoring systems and available condition rating data (e.g. OCA).

The contributions of this paper can be summarized as: (1) development of a new hybrid CBM approach that integrates high-fidelity FE model-based SHM with inspection data-based transition matrix for effective diagnosis, prognosis, and maintenance planning; (2) quantification of effects of uncertainty in OCA ratings on maintenance planning; (3) a new Bayesian scheme to update the error ratio in the OCA ratings; (4) surrogate modeling method to overcome the computational challenge in FE model-based SHM; and (5) application of the proposed framework to a miter gate problem.

Next, an overview of the proposed framework will be provided. Following that, the proposed framework is explained in detail.

2. Overview of proposed framework

Fig. 1 presents an overview of the proposed framework for optimal maintenance decisions for deteriorating components in miter gates. As shown in this figure, the proposed framework consists of four main modules, namely (1) failure prognosis based on OCA ratings, (2) maintenance planning, (3) damage diagnosis using physics-based simulation, and (4) integration of failure diagnosis and prognosis to achieve on-line planning and updating. These four modules are systematically integrated together to perform two types (*static* and *dynamic*) of optimal maintenance decisions for miter gates.

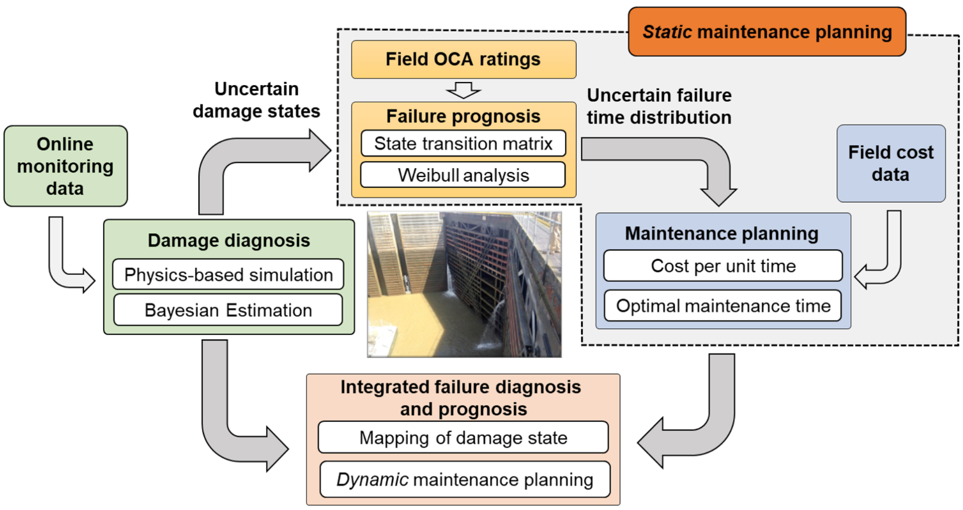

Figure 1: Overview of proposed framework for optimal maintenance decisions for deteriorating components in miter gates

The term *static* refers to the inability to update the current or future state based on the changes that a component of the system undergoes. The static maintenance planning is only based on the field OCA ratings from a large population of miter gates. The obtained maintenance decisions are therefore general to the population of miter gates and are not specific for a specific gate. Thus, the maintenance planning may not be truly optimal for a specific gate. For the static maintenance planning, there are several uncertainties to be addressed, such as how to justify a maintenance decision and how to deal with the uncertainty in the OCA rating due to *incorrect rating assignments*, i.e., ratings due to protocols are sometimes given to components even when they are not inspected.

Many miter gates are equipped with sensors which can collect strain measurement. data in real time, e.g., the SMART Gate program mentioned earlier [3]. Based on the online monitoring data and the high-fidelity physics-based simulations, the damage condition is estimated using Bayesian methods. The real-time damage diagnosis provides damage information at individual gate level, which offers an opportunity to achieve optimal maintenance planning and dynamic maintenance decisions. The integration of failure diagnosis and prognosis (as shown in Fig. 1) faces several challenges. For instance, the high-fidelity physics-based simulation model is computationally expensive, which makes Bayesian damage estimation challenging; the OCA ratings are highly abstracted and are assigned at a different time scale than the online monitoring system. The proposed framework tackles the above challenges by using the information from field OCA ratings, physics-based simulation, and online monitoring data.

Each of the following sections explains in detail the four modules mentioned earlier. Section 3 and 4 describe the static maintenance planning based only on the field OCA ratings from a large population of miter gates. Section 5 and 6 describe the formulation and application, respectively, of the dynamic maintenance planning based on the integration of prognosis models (i.e. physics-based FE model) and historical inspection data (i.e. field OCA ratings). More specially, Section 5 explains the damage diagnosis using physics-based model updating using two different degradation models (i.e. state equation) and formulates the integration of failure diagnosis, Bayesian updating of the error ratio of the OCA ratings based on damage diagnosis, and prognosis to achieve on-line planning and updating. Section 6 describes a real-world application example of the framework described in Section 5.

3. Failure prognosis based on OCA ratings

3.1 Deriving a transition matrix from OCA ratings

The USACE Asset Management team oversees the OCA process to assess structural component deficiencies by giving a category rating based on a condition and performance criteria. The ratings are classified as *A* (Excellent), *B* (Good), *C* (Fair), *D* (Poor), *F* (Failing) and *CF* (Completely Failed). More detailed definitions and discussion may be found in [2]. A transition matrix **P** (see Eq. (1)) is defined as a square matrix with nonnegative values that represents how some process "transitions" from one state to the next. In this application, an inspected OCA rating at time *t*, $I_{i,t}$, (which represents the OCA rating is *i* at time *t*, with *i*=1…6, corresponding to the 6 letter ratings specified above), will transition to inspected state at time *t*+1, $I_{j,t+1}, j=1...6$, according to

$$\mathbf{P} = P\left(I_{j,t+1} \middle| I_{i,t}\right) = \begin{bmatrix} P\left(A_{t+1} \middle| A_t\right) & \cdots & P\left(CF_{t+1} \middle| A_t\right) \\ \vdots & \ddots & \vdots \\ P\left(A_{t+1} \middle| CF_t\right) & \cdots & P\left(CF_{t+1} \middle| CF_t\right) \end{bmatrix}, \forall i, j = 1, \cdots, 6. \qquad (1)$$

Based on an OCA database, the number of times that a component transitioned from one rating category to another (as determined by engineering expert elicitation) over a given inspection time step was determined to generate the rating transition matrix. Each value in the transition matrix represents a conditional probability, and the sum of each row equals unity after normalizing the counts. Only the upper triangular components were considered to simulate component deterioration; the lower triangular components would represent improvements or repairs (transitions from a worse condition to a better condition), and for the purposes of this analysis, they were ignored. Fig. 2 shows the overall process for generating this one-step transition matrix **P**. The foundational data used to generate the counts were obtained from the OCA ratings database for navigation locks corresponding from January 2010 to June 2018, which was provided by USACE personnel.

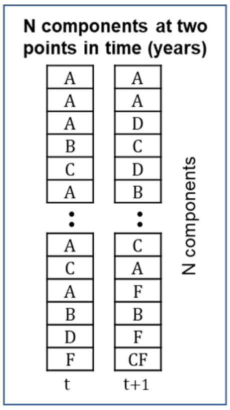

Rating	A_{t+1}	B_{t+1}	C_{t+1}	D_{t+1}	F_{t+1}	CF_{t+1}
A_t	2513	689	17	7	6	8
B_t	0	125129*($B_{inspected}/B_{total}$)	1186	469	214	70
C_t	0	0	3275	447	25	18
D_t	0	0	0	1102	59	11
F_t	0	0	0	0	813	127
CF_t	0	0	0	0	0	199

$\mathbf{P} = P\left(I_{j,t+1} \middle| I_{i,t}\right)$, *and assume* $B_{inspected}/B_{total} = 1$

Rating	A_{t+1}	B_{t+1}	C_{t+1}	D_{t+1}	F_{t+1}	CF_{t+1}
A_t	$7.76e-1$	$2.13e-1$	$5.25e-3$	$2.16e-3$	$1.85e-3$	$2.47e-3$
B_t	0	$9.85e-1$	$9.33e-3$	$3.69e-3$	$1.68e-3$	$5.51e-4$
C_t	0	0	$8.70e-1$	$1.19e-3$	$6.64e-3$	$4.78e-3$
D_t	0	0	0	$9.40e-1$	$5.03e-2$	$9.39e-3$
F_t	0	0	0	0	$8.65e-1$	$1.35e-1$
CF_t	0	0	0	0	0	1

Figure 2: 1-step (1 year) transition matrix for quoin block components

3.2 Unreliability (failure) function using transition matrix for component reliability

A failure cumulative mass function, which can approximate the probability of failure cumulative density function, can be obtained by calculating the transition probabilities after n time steps. In this case, failure is defined to be achieving the rating "*CF*". The probability that a critical component goes from OCA rating i to OCA rating j after n inspection time steps is calculated by raising the transition matrix to the power of n,

$$P\left(I_{j,t+n} \middle| I_{i,t}\right) = \mathbf{P}^n, \forall i = 1, \cdots, 6; \; j \geq i. \tag{2}$$

The conditional probability n-step transition matrix Eq. (1) can then be used to transition some initial OCA rating probabilities for each rating to the state probabilities n time steps later, or

$$P(\mathbf{I}_n) = [P\left(I_{1,n}\right), P\left(I_{2,n}\right), P\left(I_{3,n}\right), P\left(I_{4,n}\right), P\left(I_{5,n}\right), P\left(I_{6,n}\right)] = P(\mathbf{I}_0) \cdot \mathbf{P}^n, \tag{3}$$

where $P(I_{i,n}), i=1...6$, is the predicted OCA rating at time t_n, and $P(\mathbf{I}_0)$ is the initial inspected OCA rating probability, i.e.,

$$P(\mathbf{I}_0) \equiv \left[P(A_0), P(B_0), P(C_0), P(D_0), P(F_0), P(CF_0)\right]. \tag{4}$$

Fig. 3 shows the unreliability function, $F(t)$, of the quoin block component with the component age in years with the initial state probability specified as $P(\mathbf{I}_0) = [1, 0, ..., 0]$, i.e., the gate begins its OCA rating fully in rating "*A*". This is a reasonable assumption, but any initial OCA rating could be specified if other information is known, e.g., some initial degradation is possibly present at the initial time.

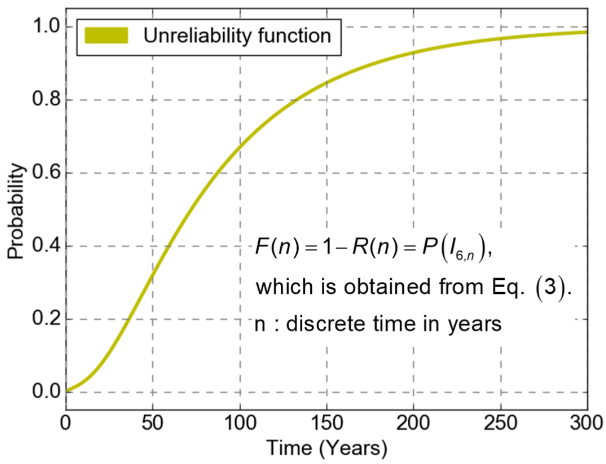

Figure 3: Unreliability function of quoin block component [34]

4. Static Optimal Maintenance Decision of Miter Gates Based on OCA Ratings

4.1. Failure time distribution modeling via Weibull analysis

The predictions about the life (i.e. reliability) of any component over time t in a structure may be fit to a Weibull distribution [9], which is commonly used in life cycle analysis. The reliability function, $R(t)$, based on the Weibull distribution is:

$$R(t) = e^{-\left(\frac{t}{\eta}\right)^{\beta}}, \tag{5}$$

where $R(t)$, β, and η are the reliability, shape parameter, and characteristic life (scale parameter), respectively. The shape parameter β must be greater than 1.0 to justify preventive maintenance due to wear out failures [4,35]. The characteristic life (or scale parameter) η represents the point in time when there is a 63.2% (when $t=\eta$ in Eq. (6)) chance of failure of the component. The corresponding failure time distribution, $F(t)$, is given by

$$F(t) = 1 - R(t) = 1 - e^{-\left(\frac{t}{\eta}\right)^{\beta}}. \quad (6)$$

For the locks and dams comprising the USACE infrastructure portfolio, the typical Periodic Inspection (PI) of the lock and dam varies from every year to occurring to a maximum of every 5 years [36]. However, the dewatering of a lock is much less frequent, often spanning multiple PI intervals. Therefore, unless there is evidence of degradation of a component that cannot be inspected, it is given a "*B*" rating. If a component was previously given something less than a "*B*" rating, and it is known that no work has been performed, the rating is carried over. Thus, many of the given "*B*" ratings are not the result of an actual inspection; this is particularly true for any component that is submerged underwater. Based on direct communication with USACE personnel, this is true for all components that are "unable to be inspected at that time, which is essentially the innocent until proven guilty mindset". After analyzing the data, it was clear that the counts remaining at B after 1 year were very large (see counts of staying at B in Figure 2). Also, it was noted that many historical OCA ratings of quoin block components didn't transition all the way from A to CF. Sometimes, the components were replaced/repaired before passing to C, D or F (or they just simply not recorded). Therefore, after discussing with USACE engineers, the source of uncertainty of the B ratings needs to be accounted for in the failure time analysis and maintenance planning.

Fig. 4 shows how the unreliability function, *F(t)*, changes when the transition matrix changes due to the uncertainty associated in the states remaining at "*B*" as explained before.

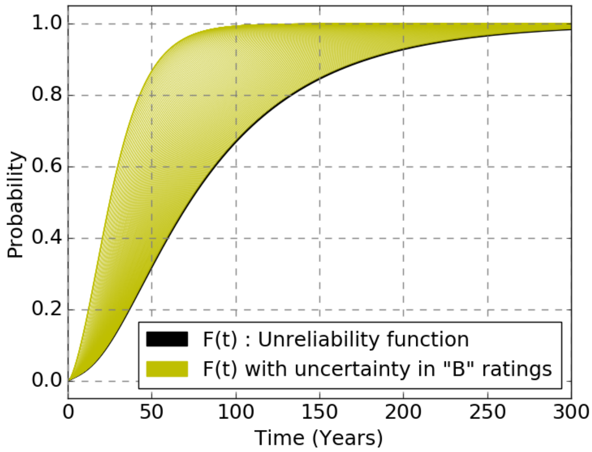

Figure 4: Unreliability function considering uncertainty in the condition rating protocol

The variability in the unreliability function was obtained by considering that the counts of remaining in state "*B*" that corresponded to an actual inspection was some ratio of the total counts reported (i.e., $B_{\text{inspected}}/B_{\text{total}}$ varies from 0 to 1).

4.2. Static optimal maintenance based on failure prognosis

Based on the unreliability function *F(t)*, the optimal maintenance time can be found by minimizing the cost function proposed by [10] to find the cost per unit of time (*CPUT*) of performing preventive maintenance at time *t* (in years) as follows:

$$CPUT(t) = \frac{C_p[1-F(t)]+C_u[F(t)]}{\int_{s=0}^{s=t}[1-F(s)]ds}, \quad (7)$$

where C_p is the preventative action cost, and C_u is the unplanned action cost. The denominator of Eq. (7) represent mean time between maintenance actions. Note that Eq. (12) has more meaning when the cost ratios, C_u / C_p, are considerably greater than 1, otherwise the numerator would behave as a constant function. Fig. 5 shows the *CPUT* computed for different cost ratios C_u / C_p, without considering the previously discussed uncertainty in the "*B*" ratings. For some miter gate, it was suggested by USACE personnel that the corresponding cost ratio is close to 5 based on cost data from lock 14 (located in the Arkansas river), which would result in a $t_{optimal}$ of about 48 years implied by Fig.5 if that were the case.

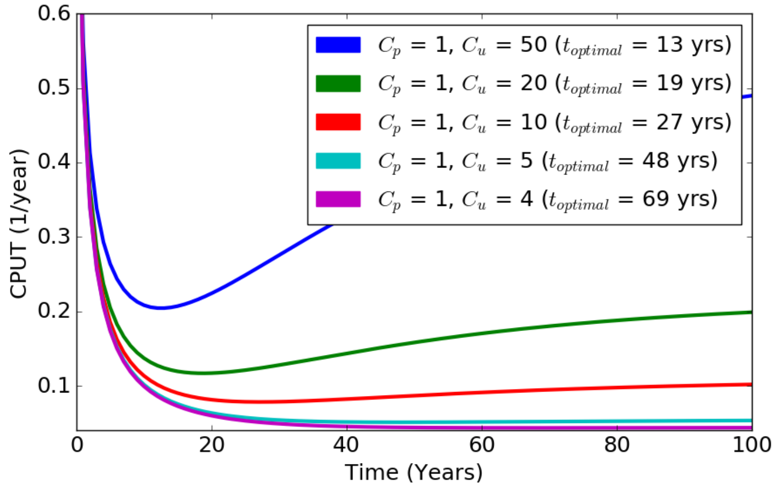

Figure 5: *CPUT* based on transition matrix with $B_{inspected}/B_{total} = 1$.

To understand the advantage and cost savings, the CPUT value at the optimal value is compared with the CPUT at other repair/replacement times, which can represent the average time that USACE regularly performs maintenance on quoin blocks. Fig. 6 shows the percentage savings using the optimal maintenance as a function of the average actual maintence time cycle. Note that if the actual maintenance time is already at its optimum, the percentage of savings is equal to 0%.

Fig. 7 shows the *CPUT* computed for different cost ratios when considering the uncertainty in the "*B*" rating in a given year. The results clearly show a lot of variability in the *CPUT*, and consequently in the optimal time to perform maintenance (i.e., the time when *CPUT* is minimized). For example, the minimum *CPUT* varies from 0.05 to 0.15 for $C_u / C_p = 5$, which is an increment of 200%. Note that the variability is larger as the cost ratio increases.

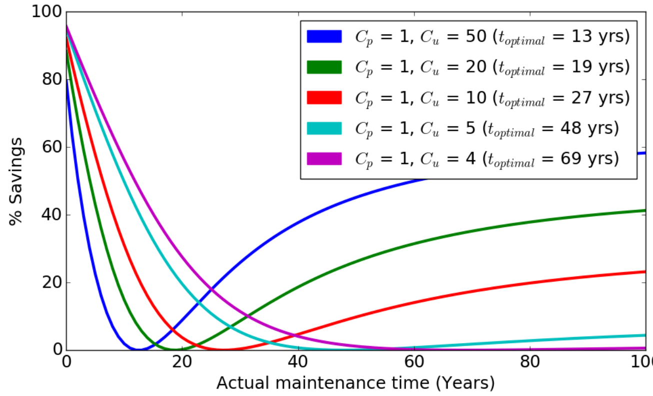

Figure 6: % Savings based on actual maintenance time

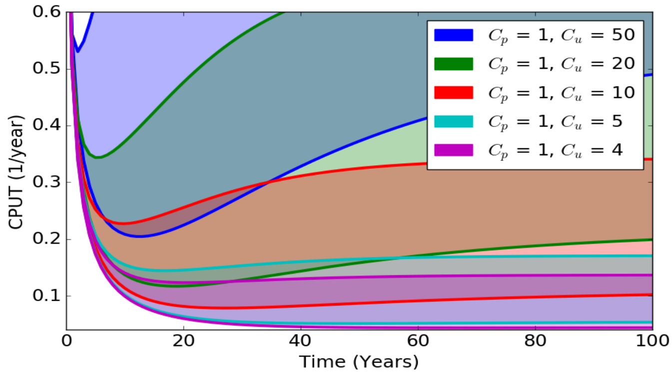

Figure 7: CPUT with $B_{\text{inspected}}/B_{\text{total}}$ from 0 (upper curves) to 1 (lower curves).

Fig. 8 shows the variability in the optimal maintenance time (between 16 and 48 years) when the cost ratio is equal to 5 (the USACE miter gate case). The variability is more pronounced when the cost ratio is small as shown in Fig. 9. The modal values at the ends represent the $t_{optimal}$ (at minimum CPUT) when $B_{\text{inspected}}/B_{\text{total}}$ approaches to 0 and 1 in the left and right end respectively. The reason is because as the $B_{\text{inspected}}$ (due to $B_{\text{inspected}}/B_{\text{total}} = 1$) approaches a large value, the normalized value in the transition matrix is still a large value. In other words, the transition probability, $P\left(B_{t+1}|B_t\right)$, is closer to 1 and larger relatively to the other transition probabilities from B_t (i.e. $P\left(A_{t+1}|B_t\right)$, $P\left(C_{t+1}|B_t\right)$, $P\left(D_{t+1}|B_t\right)$, $P\left(F_{t+1}|B_t\right)$and $P\left(CF_{t+1}|B_t\right)$). Therefore, the normalized values in the transition matrix do not change as much, and consequently the $t_{optimal}$ does not change as much. Similar behavior is observed when $B_{\text{inspected}}$ (due to $B_{\text{inspected}}/B_{\text{total}} = 0$)

approaches to 0. Except that, $P\left(B_{t+1}\middle|B_t\right)$, is closer to 0 and smaller relative to the other transition probabilities.

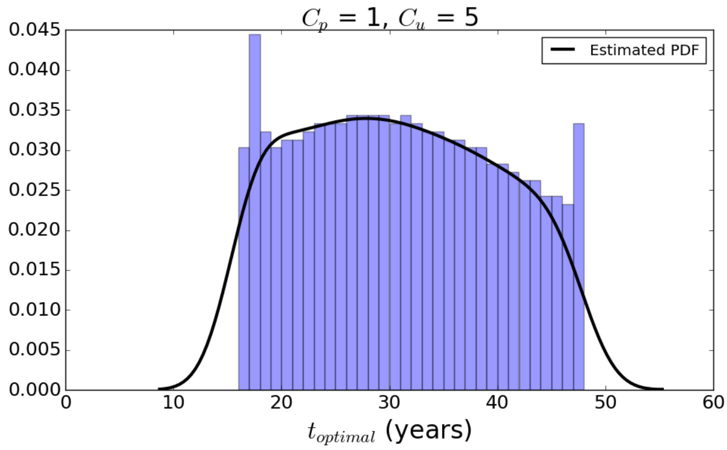

Figure 8: Variability in optimal maintenance time for $C_u/C_p = 5$

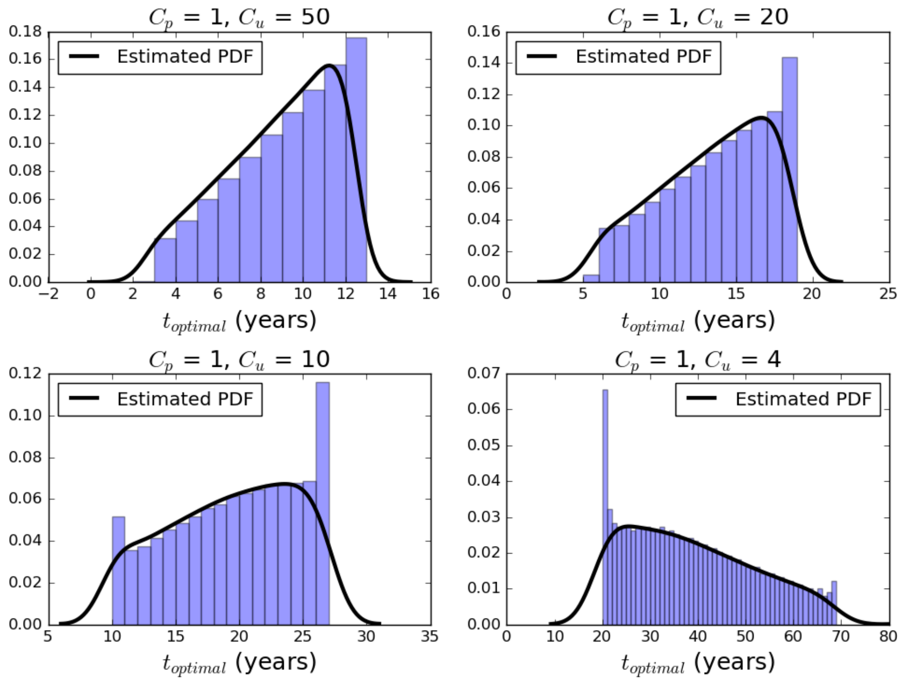

Figure 9: Variability in optimal maintenance time for different cost ratios

Table 1 summarizes the statistics of the time variability shown in Figures 8 and 9. Based on these statistics, the average optimal maintenance time considering only the reliability of quoin block in miter gates would be almost 31 years. As mentioned earlier, the cost ratio for lock 14 is close to 5, so an interpolation can be made for the optimal maintenance between 4 and 5 if needed. Also, the reason why larger cost ratio values (e.g. 10, 20 and 50) were considered is because miter gates in the Mississippi river or other rivers would have higher traffic demands than lock 14. In other words, the downtime cost for these gates will logically be increased (C_u would be larger).

Table 1: Optimal maintenance time (years) statistics

Cp/Cu	Mean	SD	Max	Min
50	8.82	2.59	13	2
20	13.47	3.60	19	5
10	19.27	4.99	27	10
5	30.75	9.09	48	16
4	38.52	13.48	69	20

Up to this point the maintenance planning has been depending only on the historical inspection data (i.e. field OCA ratings). However, current state (or damage) estimation can enable dynamic decision making, which may lead to reduced lifecycle cost. To achieve this, Sec. 5 proposes the integration of diagnostic models (i.e. physics-based FE modeling) and historical inspection data (i.e. field OCA ratings). As mentioned before, the following section formulates the integration of failure diagnosis and prognosis to achieve on-line planning and updating.

5. Integration of Damage Diagnosis and Failure Prognosis for Dynamic Maintenance Planning of Miter Gates

As demonstrated in Sec. 4, optimal maintenance highly depends on the evolution of the damage, e.g., how fast the probability of "*CF*" changes with time. Ideally, a degradation model of every damage level present in every component in the gate would facilitate the maintenance decision-making process. However, sometimes there is not a clear understanding of how the damage evolves with time. For example, such is the case with miter gates, where it is not understood how the bearing gaps change in time. This is one motivation for integrating SHM with the Markov transition matrix. Figure 10 shows more details of the proposed framework to integrate SHM with the Markov transition matrix. As shown in this figure, the proposed framework first estimates the damage sate (i.e. gap length) using online SHM data. The estimated gap length is then used to update the error ratio in the "B" ratings. Based on that, the Markov transition matrix is updated, which will be used for failure prognosis and dynamical optimal maintenance planning. In what follows, each element of the proposed framework is explained in detail.

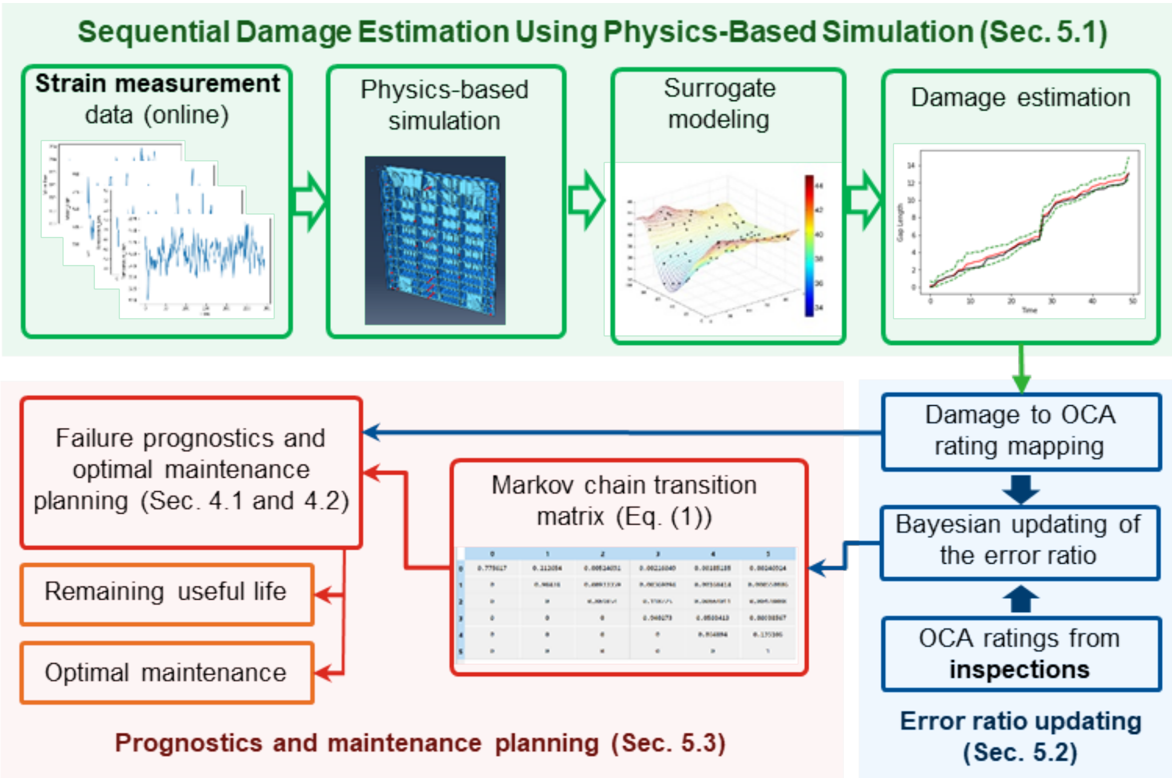

Figure 10: Overview of the proposed framework

5.1 Sequential damage estimation using physics-based simulation

Let $\mathbf{s}_i = [s_{i1}, s_{i2}, \cdots, s_{iN_S}]$ be the strain measurement data at time step t_i, where N_S is the number of strain sensors, the posterior probability density function of the gap length h_n at time step t_n conditioned on strain measurements $\mathbf{s}_{1:n} \triangleq \{\mathbf{s}_1, \mathbf{s}_2, \cdots, \mathbf{s}_n\}$ collected up to t_n is given by

$$f(h_n \mid \mathbf{s}_{1:n}) = \frac{f(\mathbf{s}_n \mid h_n) f(h_n \mid \mathbf{s}_{1:n-1})}{\int f(\mathbf{s}_n \mid h_n) f(h_n \mid \mathbf{s}_{1:n-1}) dh_n} \propto f(\mathbf{s}_n \mid h_n) f(h_n \mid \mathbf{s}_{1:n-1}), \quad (8)$$

where $f(h_n \mid \mathbf{s}_{1:n-1})$ is given by

$$f(h_n \mid \mathbf{s}_{1:n-1}) = \int f(h_n \mid h_{n-1}) f(h_{n-1} \mid \mathbf{s}_{1:n-1}) dh_{n-1}, \tag{9}$$

with $f(\mathbf{s}_n \mid h_n)$ being the likelihood function (from the measurement equation) of observing $\mathbf{s}_n$ for given h_n at time step t_n, and $f(h_n \mid h_{n-1})$ is the PDF of h_n for a given h_{n-1} obtained from the state equation which describes the damage evolution over time.

As illustrated in Fig. 10, the physics-based simulation model is employed as the measurement equation in this paper. The likelihood function $f(\mathbf{s}_n \mid h_n)$, assuming that the observations $\mathbf{s}_n$ are statistically independent, is computed by

$$f(\mathbf{s}_n \mid h_n) = \prod_{j=1}^{N_S} \phi\left(\frac{s_{nj} - \mu_{sj}(h_n)}{\sigma_\varepsilon}\right), \tag{10}$$

where $\phi(\cdot)$ is the PDF of the standard normal distribution, σ_ε is the standard deviation of the observation noise, and $\mu_{sj}(h_n)$ is the mean strain response prediction at the location of the *j*-th sensor obtained from the physics-based simulation.

Since the physics-based computer simulation model is used to predict $\mu_{sj}(h_n), \forall j = 1, 2, \cdots, N_S$ and the likelihood function $f(\mathbf{s}_n \mid h_n)$ needs to be evaluated numerous times during the sequential damage estimation, this is computationally burdensome. To address this challenge, a surrogate model is constructed for the strain response at N_S strain locations as $\mathbf{s} = [s^{(1)}, s^{(2)}, \cdots, s^{(N_S)}] = \hat{g}_h(\mathbf{x})$, where $s^{(j)}, j = 1, 2, \cdots, N_S$ is the strain response prediction at the *j*-th sensor location and $\mathbf{x} = [h, \boldsymbol{\theta}]$ including the gap length (h) and other model parameters ($\boldsymbol{\theta}$) such as hydrostatic and thermal loads applied to miter gates.

To build such a surrogate model and tackle the challenge of the high-dimensional output during surrogate modelling, *N* training points are first generated for $\mathbf{x}$ and are denoted as $\mathbf{x}_t \triangleq \{\mathbf{x}_1, \mathbf{x}_2, \cdots, \mathbf{x}_N\}$. From physics-based simulations, a data matrix of the strain responses for *N* training points is obtained as below

$$\mathbf{w} = [\mathbf{w}(\mathbf{x}_1), \mathbf{w}(\mathbf{x}_2), \ldots, \mathbf{w}(\mathbf{x}_N)]^T \\ = \begin{bmatrix} w(1, \mathbf{x}_1) & w(1, \mathbf{x}_2) & \cdots & w(1, \mathbf{x}_N) \\ w(2, \mathbf{x}_1) & w(2, \mathbf{x}_2) & \cdots & w(2, \mathbf{x}_N) \\ \vdots & \vdots & \ddots & \vdots \\ w(N_S, \mathbf{x}_1) & w(N_S, \mathbf{x}_2) & \cdots & w(N_S, \mathbf{x}_N) \end{bmatrix}^T \in \mathbb{R}^{N \times N_S}, \tag{11}$$

where $\mathbf{w}(\mathbf{x}_i) = [w(1, \mathbf{x}_i), w(2, \mathbf{x}_i), \cdots, w(N_S, \mathbf{x}_i)]^T \in \mathbb{R}^{N_S \times 1}$ is the strain response with inputs $\mathbf{x}_i, \forall i = 1, 2, \cdots, N_S$, $w(j, \mathbf{x}_i)$ is the strain response at the *j*-th sensor location, and N_S is the number of sensors as discussed before.

The data matrix $\mathbf{w}$ shown above is then compressed using singular value decomposition (SVD) as

$$\mathbf{w} = \mathbf{VMU}^T, \tag{12}$$

where $\mathbf{V}$ is a $N \times N$ orthogonal matrix, $\mathbf{U}$ is a $N_S \times N_S$ orthogonal matrix and $\mathbf{M}$ is a $N \times N_S$ rectangular diagonal matrix with non-negative real numbers $\boldsymbol{\lambda} = [\lambda_1, \lambda_2, \ldots, \lambda_k]$ on the diagonal, in which k is minimum of N and N_S.

Defining another matrix as $\boldsymbol{\gamma} = \mathbf{VM}$, the original data matrix $\mathbf{w}$ can be reconstructed

$$\mathbf{w}(\cdot, \mathbf{x}_i)^T \approx \sum_{j=1}^{r} \gamma_{ij} \mathbf{U}_j, \tag{13}$$

where $\boldsymbol{\gamma}_{i:} = [\gamma_{i1}, \gamma_{i2}, \cdots, \gamma_{ir}]$ is the *i*-th row of $\boldsymbol{\gamma}$, $\mathbf{w}(\cdot, \mathbf{x}_i)^T$ is the *i*-th row of $\mathbf{w}$, γ_{ij} is the element of $\boldsymbol{\gamma}$ at *i*-th row and *j*-th column, $\mathbf{U}_j$ is the *j*-th important feature vector used to approximate $\mathbf{w}$, and *r* is the number of features retained in the decomposition.

Eq. (13) shows that the variation in the high-dimensional response across the design domain mainly comes from the variation in $\boldsymbol{\gamma}_{i:} = [\gamma_1(\mathbf{x}_i), \gamma_2(\mathbf{x}_i), \cdots, \gamma_r(\mathbf{x}_i)]$, which denotes the value of γ for *i*-th training point. With the training points of

$\boldsymbol{\gamma}_{i:} = [\gamma_1(\mathbf{x}_i), \gamma_2(\mathbf{x}_i), \cdots, \gamma_r(\mathbf{x}_i)]$ and $\mathbf{x}_i$, $i = 1, 2, \cdots, N$, a surrogate models is constructed for $\gamma_1, \gamma_2, \cdots,$ and γ_r as $\hat{\gamma}_j = \hat{g}_j(\mathbf{x}), \forall j = 1, 2, \cdots, r$ using the Kriging surrogate modelling method. In Kriging surrogate modelling, $\hat{\gamma}_j = \hat{g}_j(\mathbf{x})$ is approximated as

$$\hat{\gamma}_j = \hat{g}_j(\mathbf{x}) = \mathbf{f}(\mathbf{x})^T \boldsymbol{\alpha} + Z(\mathbf{x}), \tag{14}$$

where $\boldsymbol{\alpha}$ are coefficients of the trend function $\mathbf{f}(\mathbf{x})^T$, and $Z(\mathbf{x}) \sim N(0, \sigma_{GP}^2 \rho(\bullet, \bullet))$ is a stationary Gaussian process with correlation function $\rho(\bullet, \bullet)$ between the responses at any two points given by

$$\rho(\mathbf{x}, \mathbf{x}') = \exp\left\{-\sum_{l=1}^{N_V} \omega_l (x_l - x_l')^2\right\}, \tag{15}$$

in which N_V is the number of variables, and $\boldsymbol{\omega} = (\omega_1, \ldots, \omega_{N_V})^T$ is a vector of roughness parameters.

The hyper-parameters $\boldsymbol{\upsilon} = \left(\boldsymbol{\alpha}, \sigma_{GP}^2, \boldsymbol{\omega}\right)$ can be estimated using the maximum likelihood estimation method (used in this paper) or the least-squares method. After the estimation of the hyper-parameters $\boldsymbol{\upsilon}$, for any given inputs $\mathbf{x}$, the GP prediction is a Gaussian random variable given by

$$\hat{\gamma}_j = \hat{g}_j(\mathbf{x}) \sim N(\mu_j(\mathbf{x}), \sigma_j^2(\mathbf{x})), \forall j = 1, 2, \cdots, r, \tag{16}$$

where $\mu_j(\mathbf{x})$ and $\sigma_j^2(\mathbf{x})$ are respectively the mean and variance of the prediction of γ_j at input $\mathbf{x}$. Combining Eqs. (13) and (16), the strain response in the original space (i.e. strain at .N_s. locations) of the kriging surrogate model can be expressed as

$$[\hat{w}(1, \mathbf{x}), \hat{w}(2, \mathbf{x}), \cdots, \hat{w}(N_s, \mathbf{x})] = \sum_{j=1}^{r} \hat{g}_j(\mathbf{x}) \mathbf{U}_j. \tag{17}$$

For any given $\mathbf{x} = [h, \boldsymbol{\theta}]$, the prediction of the strain response in the original space is given by

$$\hat{w}(i, \mathbf{x}) \sim N(\mu_w(i, \mathbf{x}), \sigma_w^2(i, \mathbf{x})), \forall i = 1, 2, \cdots, N_S, \tag{18}$$

where $\mu_w(i, \mathbf{x}) = \sum_{j=1}^{r} \mu_j(\mathbf{x}) U_j(i)$ and $\sigma_w(i, \mathbf{x}) = \sqrt{\sum_{i=1}^{r} \sigma_j^2(\mathbf{x}) U_j^2(i)}$. The covariance of $\hat{w}(i, \mathbf{x})$ and $\hat{w}(k, \mathbf{x})$ is given by

$$\Sigma_{ik} = \sum_{j=1}^{r} \sigma_j^2(\mathbf{x}) U_j(i) U_j(k), \forall i, k = 1, 2, \cdots, N_S. \tag{19}$$

For sensor locations $i = k$, after considering uncorrelated and unbiased observation noise, the diagonal entries of the covariance matrix become

$$\Sigma_{ii} = \sum_{j=1}^{r} \sigma_j^2(\mathbf{x}) U_j^2(i) + \sigma_\varepsilon^2, \forall i = 1, 2, \cdots, N_S. \tag{20}$$

After substituting the original physics-based simulation with the surrogate model as discussed above, the likelihood function $f(\mathbf{s}_n \mid h_n)$ in the sequential damage estimation is computed by

$$f(\mathbf{s}_n \mid h_n) = \frac{\exp\left(-0.5(\mathbf{s}_n - \boldsymbol{\mu}_w)^T \boldsymbol{\Sigma}^{-1} (\mathbf{s}_n - \boldsymbol{\mu}_w)\right)}{\sqrt{(2\pi)^{N_S} \left|\boldsymbol{\Sigma}\right|}}, \tag{21}$$

where the mean and covariance terms are given by $\boldsymbol{\mu}_w = [\mu_w(1, \mathbf{x}), \mu_w(2, \mathbf{x}), \cdots, \mu_w(N_S, \mathbf{x})]$ and $\boldsymbol{\Sigma} = \{\Sigma_{ik}, \forall i, k = 1, 2, \cdots, N_S\}$, computed by plugging h_n into Eqs. (16) and (17).

From Eqs. (10) to (21), the computation of $f(\mathbf{s}_n \mid h_n)$ has been discussed in the sequential damage estimation using a physics-based simulation model. As indicated in Eqs. (8) and (9), an important step in the sequential damage estimation is the evaluation of $f(h_n \mid h_{n-1})$, which is usually based on the state equation of the damage propagation. As mentioned previously, however, the degradation mechanism of the miter gate is complicated and not fully understood; there is no appropriate physics-based degradation model available that can adequately describe the growth of the gap. The only known information is that the gap will grow over time (no self-repair/replace). In this situation, the following minimally informed state equation is employed

$$h_n = h_{n-1} + \varepsilon_h, \tag{22}$$

in which ε_h is a sufficiently large process noise term that imposes random gap growth over time, i.e., gap growth is a random walk. Since the gap can only grow over time, a Weibull process noise with a shape parameter of 0.5 and a scale parameter of 1.2 is used in this paper which is able to cover a wide range (from 0 to 228 cm) of gap growth rate.

By recursively implementing Eqs. (8) and (9), the miter gate gap length is estimated based on the online strain measurement data. In this paper, the particle filtering (PF) method [37] is employed to perform the sequential damage estimation through the online strain measurement and the physics-based simulation. Let the particles from the (n-1)-th time step after performing prediction using the state equation be $\mathbf{h}_n = [h_{n1}, h_{n2}, \cdots, h_{nN_p}]$, where N_p is the number of particles in particle filtering, the posterior distribution at the n-th time step is obtained by resampling the particles according to the following weights

$$\chi_i = \frac{f(\mathbf{s}_n \mid h_{ni})}{\sum_{i=1}^{N_p} f(\mathbf{s}_n \mid h_{ni})}, \forall i = 1, 2, \cdots, N_p \tag{23}$$

where $f(\mathbf{s}_n \mid h_{ni})$ is obtained by plugging h_{ni} into Eq. (21).

As being shown in Sec. 6.2, the state equation given in Eq. (22) allows for effective damage estimation through sequential Bayesian inference. Let the distribution parameters of ε_h be λ_h and κ_h, where λ_h is the scale parameter of Weibull distribution and κ_h is the shape parameter of the distribution, if the state equation given in Eq. (22) is used for prognosis, the gap length h_m after m months ($m > 30$, prognosis over 30 months) can be approximated as a normal distribution as below according to the central limit theorem

$$H_m \sim N(h_n + m\mu_\varepsilon, m\sigma_\varepsilon^2), \tag{24}$$

where H_m stands for a random gap length, h_m is a specific realization of H_m, h_n is the current gap length, $\mu_\varepsilon = \lambda_h \Gamma(1+1/\kappa_h)$ and $\sigma_\varepsilon^2 = \lambda_h^2 \left[\Gamma(1+2/\kappa_h) - \left(\Gamma(1+1/\kappa_h) \right)^2 \right]$ are respectively the mean and variance of ε_h.

The probability that the remaining useful life (RUL), T_R, is less than a specific value q, is then given by

$$\Pr\{T_R < q\} = \Pr\{h_q > h_e\} = 1 - \Phi\left(\frac{h_e - (h_n + q\mu_\varepsilon)}{\sqrt{q}\sigma_\varepsilon} \right), \tag{25}$$

in which h_e is the gap failure threshold (i.e., 381 cm. this paper).

Based on the above equation, the $(1-\alpha)$ confidence interval of the RUL conditioned on the current gap length h_n is derived as

$$\left[T_{1-\alpha/2}, T_{\alpha/2} \mid h_n \right] = \frac{2\mu_\varepsilon (h_e - h_n) + (\Phi^{-1}(\alpha/2))^2 \sigma_\varepsilon^2}{2\mu_\varepsilon^2} \pm \frac{T_\varepsilon}{2\mu_\varepsilon^2}, \tag{26}$$

where T_ε is given by

$$T_\varepsilon = \sqrt{\left[2\mu_\varepsilon (h_e - h_n) + (\Phi^{-1}(\alpha/2))^2 \sigma_\varepsilon^2 \right]^2 - 4\mu_\varepsilon^2 (h_e - h_n)^2}. \tag{27}$$

The unconditional $(1-\alpha)$ confidence interval of the RUL can then be computed by

$$T_{\alpha/2} = \int f(h_n \mid \mathbf{s}_{1:n}) \left[T_{\alpha/2} \mid h_n \right] dh_n, \tag{28}$$

in which $f(h_n \mid \mathbf{s}_{1:n})$ is the posterior distribution of h_n obtained from the damage diagnosis.

If the state equation given in Eq. (22) is accurate, the above equations allow to analytically estimate the RUL. Due to the large process noise ε_h and the discrepancy between the state equation and the underlying unknown degradation model, Eq. (22) could lead to large error in the remaining useful life (RUL) estimation when it is applied to the failure prognosis (see the result in Sec. 6.3). Therefore, the state equation Eq. (22)

cannot be used for optimal maintenance planning. Motivated to overcome this limitation, the physics-based damage estimation is integrated with the Markov transition matrix in the subsequent sections for (1) updating of the error ratios in the "B" ratings, and (2) failure prognosis of the miter gate based on SHM and transition matrix.

5.2 Updating of "B" ratings error ratio based on online damage estimation

As been shown in Secs.4.1 and 4.2, the uncertainty in $B_{\text{inspected}}/B_{\text{total}}$ could significantly affect the failure prognosis results and maintenance planning. In order to reduce the uncertainty using the damage estimation technique developed in Sec. 5.1, a mapping of the estimated gap length h_n on to an OCA rating is performed as follows:

$$I_n = I_{OCA}(h_n) = \begin{cases} I_{1,n}, & h_n \in [e_0, e_1) \\ I_{2,n}, & h_n \in [e_1, e_2) \\ I_{3,n}, & h_n \in [e_2, e_3) \\ I_{4,n}, & h_n \in [e_3, e_4) \\ I_{5,n}, & h_n \in [e_4, e_5) \\ I_{6,n}, & h_n \geq e_5 \end{cases}, \tag{29}$$

where $I_n = I_{OCA}(h_n)$ is a function that maps a gap length h_n to an OCA rating I_n at time step t_n, and $e_j, j = 0, 1, \cdots, 5$ are the gap length thresholds used to partition the gap domain into OCA ratings.

In order to use the estimated OCA ratings to update the error ratio of the "B" ratings, the variable $B_{\text{inspected}}/B_{\text{total}}$ is defined as $\gamma = B_{\text{inspected}} / B_{\text{total}}$. γ is then updated using Bayesian method based on the damage estimation as follows

$$f_{\gamma|I}(\gamma \mid \mathbf{I}_{1:n}) = \frac{f_{I|\gamma}(\mathbf{I}_{1:n} \mid \gamma) f_{\gamma}(\gamma)}{\int f_{I|\gamma}(\mathbf{I}_{1:n} \mid \gamma) f_{\gamma}(\gamma) d\gamma} \propto f_{I|\gamma}(\mathbf{I}_{1:n} \mid \gamma) f_{\gamma}(\gamma), \tag{30}$$

in which $\mathbf{I}_{1:n} \triangleq [I_1, I_2, \cdots, I_n]$ are the estimated OCA ratings of time steps t_1 to t_n from the SHM system by mapping the estimated gap lengths into OCA ratings using Eq. (29),

$f_\gamma(\gamma)$ is the prior distribution of γ, the non-informative uniform distribution $\gamma \sim \mathrm{U}(0,1)$ is used in this paper (i.e. $f_\gamma(\gamma)=1$), and $f_I(\mathbf{I}_{1:n} \mid \gamma)$ is the likelihood function of observing $\mathbf{I}_{1:n}$ for given γ.

Since the estimated $\mathbf{I}_{1:n} \triangleq [I_1, I_2, \cdots, I_n]$ are uncertain due to the uncertainty in $h_i, i=1,2,\cdots,n$, Eq. (30) is rewritten as follows by considering the uncertainty in $\mathbf{I}_{1:n}$

$$f_{\gamma|I}(\gamma \mid \mathbf{I}_{1:n}) = \sum_{\mathbf{I}_{obs}} f_{\gamma|I}(\gamma \mid \mathbf{I}_{obs}) P\{\mathbf{I}_{1:n} = \mathbf{I}_{obs}\}, \tag{31}$$

where $\mathbf{I}_{obs}$ is an observation realization of $\mathbf{I}_{1:n} \triangleq [I_1, I_2, \cdots, I_n]$ obtained from the physics-based damage estimation in Sec. 5.1, and $f_{\gamma|I}(\gamma \mid \mathbf{I}_{obs})$ is given by

$$f_{\gamma|I}(\gamma \mid \mathbf{I}_{obs}) \propto f_{I|\gamma}(\mathbf{I}_{obs} \mid \gamma) f_\gamma(\gamma). \tag{32}$$

Defining the posterior samples of gap length from Sec. 5.1 as h_{jk}, $\forall j=1,2,\cdots,n; k=1,2,\cdots,N_p$; (see Eq. (23) in Sec. 5.1), where N_p is the number of particles in particle filtering and h_{jk} is the *k*-th particle at time step t_j. Using the posterior samples from t_1 to t_n, Eq. (31) is approximated as

$$f_{\gamma|I}(\gamma \mid \mathbf{I}_{1:n}) \approx \frac{1}{N_p} \sum_{k=1}^{N_p} f_{\gamma|I}(\gamma \mid \mathbf{h}_{\bullet k}), \tag{33}$$

where $\mathbf{h}_{\bullet k} \triangleq [h_{1k}, h_{2k}, \cdots, h_{nk}]$ is the *k*-th realization of the gap length estimation, and $f_{\gamma|I}(\gamma \mid \mathbf{h}_{\bullet k})$ is given by

$$f_{\gamma|I}(\gamma \mid \mathbf{h}_{\bullet k}) \propto f_{I|\gamma}(\mathbf{h}_{\bullet k} \mid \gamma) f_\gamma(\gamma), \tag{34}$$

in which

$$f_{I|\gamma}(\mathbf{h}_{\bullet k} \mid \gamma) = \prod_{j=1}^{n} f_{I|\gamma}(h_{jk} \mid \gamma). \tag{35}$$

The $f_{I|\gamma}(h_{jk} \mid \gamma)$ is computed based on the OCA rating transition matrix as

$$f_{I|\gamma}(h_{jk} \mid \gamma) = P(I_{OCA}(h_{jk}), \gamma), \forall j = 1, 2, \cdots, n, \tag{36}$$

where $P(I_{OCA}(h_{jk}), \gamma)$ is an element of $\mathbf{P}_{(j)}(\gamma)$ with index of the element determined by $I_{OCA}(h_{jk})$ given in Eq. (29).

$\mathbf{P}_{(j)}(\gamma)$ is obtained using a transition matrix conditioned on γ (see Secs. 3.2 and 4.1) as follows

$$\mathbf{P}_{(j)}(\gamma) = [P(I_{1,j}, \gamma), P(I_{2,j}, \gamma), \cdots, P(I_{6,j}, \gamma)] = P(\mathbf{I}_0) \cdot \mathbf{P}_M^j(\gamma), \tag{37}$$

in which $\mathbf{P}_M^j(\gamma)$ is a modified transition matrix to account for the difference in the time scales of the SHM system and the 1-year transition matrix obtained from inspection data. For instance, in this paper the time scale of the SHM system is in months; therefore, $\mathbf{P}_M^j(\gamma) = (\mathbf{P}(\gamma))^{1/12}$ in which $\mathbf{P}(\gamma)$ is obtained by following the procedure depicted in Fig. 2 and setting $B_{\text{inspected}} / B_{\text{total}} = \gamma$.

Using Eqs. (31) through (37), the error ratio of the "B" ratings can be updated over time based on the SHM damage estimations. Next, it is discussed how to perform failure prognostics and maintenance planning based on the updating.

5.3 Failure prognosis and dynamic optimal maintenance planning

As indicated in Fig. 10, the above sequential damage estimation (using physics-based simulation in Sec. 5.1) and the updating of the error ratio (Sec. 5.2) are integrated with the transition matrix to overcome the challenge that there is no degradation model available for failure prognosis. To achieve this purpose, the probability mass function (PMF) of a certain OCA rating is computed based on the posterior distribution of the gap length obtained from physics-based damage estimation (Sec. 5.1) and the mapping from gap length to OCA rating in Eq. (29). Taking the OCA rating "$I_{i,n}$" (i.e. the OCA rating is i at time step t_n) as an example, the PMF of " $I_{i,n}$ " conditioned on the strain observations $\mathbf{s}_{1:n}$ collected up to current time step t_n, is given by

$$P(I_{i,n} \mid \mathbf{s}_{1:n}) = \Pr\left\{I_n = I_{i,n} \mid \mathbf{s}_{1:n}\right\} = \begin{cases} \int_{e_{i-1}}^{e_i} f(h_n \mid \mathbf{s}_{1:n}) dh_n, \text{if } i \le 5 \\ \int_{e_{i-1}}^{\infty} f(h_n \mid \mathbf{s}_{1:n}) dh_n, \text{otherwise} \end{cases}, \forall i = 1, \cdots, 6, \quad (38)$$

in which $\Pr\{\cdot\}$ is the probability operator and $f(h_n \mid \mathbf{s}_{1:n})$ is the posterior distribution obtained from damage estimation as discussed in Sec. 5.1.

Since particle filtering method is employed, the PMF $P(I_{i,n} \mid \mathbf{s}_{1:n})$ is approximated as

$$P(I_{i,n} \mid \mathbf{s}_{1:n}) = \Pr\left\{I_n = I_{i,n} \mid \mathbf{s}_{1:n}\right\} \approx \frac{\sum_{k=1}^{N_p} \Lambda(h_{nk})}{N_p}, \forall i = 1, \cdots, 6, \quad (39)$$

where $h_{nk}, k = 1, 2, \cdots, N_p$ are the posterior samples at t_n, $\Lambda(h_{nk}) = 1,$ if $I_{OCA}(h_{nk}) = I_{i,n}$ and $\Lambda(h_{nk}) = 0$, otherwise.

Based on the above equation, the PMF of all COA ratings conditioned on $\mathbf{s}_{1:n}$ can be expressed as

$$P(\mathbf{I}_n \mid \mathbf{s}_{1:n}) = [P(I_{1,n} \mid \mathbf{s}_{1:n}), P(I_{2,n} \mid \mathbf{s}_{1:n}), ..., P(I_{6,n} \mid \mathbf{s}_{1:n})]. \quad (40)$$

Combining Eqs. (40) and (3), the OCA rating after m time steps conditioned on current strain observations ($\mathbf{s}_{1:n}$) and given value of the error ratio γ is given by

$$P\left(\mathbf{I}_{n+m} \mid \mathbf{s}_{1:n}, \gamma\right) = P\left(\mathbf{I}_n \mid \mathbf{s}_{1:n}\right) \cdot \mathbf{P}^m(\gamma), \quad (41)$$

where $\mathbf{P}(\gamma)$ is the transition matrix given in Fig. 2 for given $B_{\text{inspected}} / B_{\text{total}} = \gamma$.

The cumulative density function (CDF) of the remaining useful life is then computed as

$$\begin{aligned}\Pr\{RUL \le m \mid \mathbf{s}_{1:n}\} &= \int \Pr\{RUL \le m \mid \mathbf{s}_{1:n}, \gamma\} f_{\gamma|I}(\gamma \mid \mathbf{I}_{1:n}) d\gamma, \\ &= \int F_{t|\mathbf{s}_{1:n}}(m, \gamma) f_{\gamma|I}(\gamma \mid \mathbf{I}_{1:n}) d\gamma, \\ &= \int P(\left[I_{n+m} \mid \mathbf{s}_{1:n}\right] = I_{6,n+m}) f_{\gamma|I}(\gamma \mid \mathbf{I}_{1:n}) d\gamma,\end{aligned} \tag{42}$$

where $F_{t|\mathbf{s}_{1:n}}(m, \gamma)$ is the failure probability in the future *m* time steps conditioned on $\mathbf{s}_{1:n}$ and γ, and $f_{\gamma|I}(\gamma \mid \mathbf{I}_{1:n})$ is the posterior distribution of γ obtained in Sec. 5.2.

With strain observations collected through the sensors, the gap length and error ratio are updated over time through the damage estimation discussed in Sec. 5.1 and the error ratio updating scheme in Sec. 5.2. The RUL is then updated through Eqs. (38) and (42). The results of a miter gate application show that integrating physics-based damage estimation and the Markov transition matrix allows for effective RUL estimate even through there is no degradation model available.

Based on the failure prognosis, the $CPUT(t)$ in the future *m* time steps conditioned on the current strain observations and an error ratio γ is given by

$$[CPUT(m) \mid \mathbf{s}_{1:n}, \gamma] = \frac{C_P[1 - F_{t|\mathbf{s}_{1:n}}(m, \gamma)] + C_U[F_{t|\mathbf{s}_{1:n}}(m, \gamma)]}{\int_0^m [1 - F_{t|\mathbf{s}_{1:n}}(\tau, \gamma)] d\tau}, \tag{43}$$

where $F_{t|\mathbf{s}_{1:n}}(\tau, \gamma)$ is the failure probability given in Eq. (42), which needs to be interpolated from discrete time steps to continuous time step to evaluate the $CPUT(t)$ for any given future time.

The expected optimal maintenance plan conditioned on current observations, $\mathbf{s}_{1:n}$, is then identified as

$$[t_{opt} \mid \mathbf{s}_{1:n}] = \int \arg\min_t \{CPUT(t) \mid \mathbf{s}_{1:n}, \gamma\} f_{\gamma|I}(\gamma \mid \mathbf{I}_{1:n}) d\gamma. \tag{44}$$

The above equation is the result of integrating SHM with the Markov transition matrix based on field OCA ratings, which allows updating the optimal maintenance plan over time. This enables for dynamic decision making and thus leads to reduced lifecycle cost. Next, a miter gate application is used to demonstrate the effectiveness of the proposed framework and investigate effects of the mapping function on the decision-making process.

6. Application to Miter Gate Failure Prognosis and Maintenance Optimization

In this section, the proposed framework is applied to an in-service USACE miter gate to demonstrate the effectiveness of the proposed prognosis and maintenance optimization.

6.1 Physics-based simulation model of miter gate

A FE model of the Greenup miter gate (Kentucky, USA) is used to understand the physics of a real-world miter gate. This model has been previously validated in the undamaged condition [5] with the available strain gage readings from the Greenup miter gate. Due to the SHM network already mounted in the Greenup miter gate [3], the effect of input parameters such as the gap length (and other parameters such as the hydrostatic and thermal loads on the gates) to the strain network is analyzed using this validated FEM model.

The Greenup gate is a relatively new gate where negligible damage (gap length) was assumed for validation purposes. Most elements in the gate are 3D linear shells elements to reduce the computational cost of such a large model. A contact-type constraint is used between the quoin block attached lock wall (denoted in orange) and the gate (denoted in gray), making this a nonlinear problem. The Lagrange multiplier method was employed to impose the contact constraint. The strain gauge locations are far from the contact area, mostly due to physical constraints in the miter gate, but this far-field location also mitigates errors due to the method employed to enforce the contact constraint. The opposite side of the lock wall uses fixed boundary conditions, and symmetry boundary conditions are used at the right end (i.e., the miter) of the gate to simulate the right leaf. Figure 11 shows the FE model of the Greenup gate and the modeling of bearing gap (enclosed area). The bearing gap (loss of contact) is modelled by removing the part of the quoin block attached to the lock wall (denoted in orange). Note that the size of the bearing gap in Figure 11 is just representative, as this will be a varying input variable to the FE model to generate "damage" data extracted from sensor locations in the gate. For more details on the quoin block mechanism, refer to Figure 8.37b in [38].

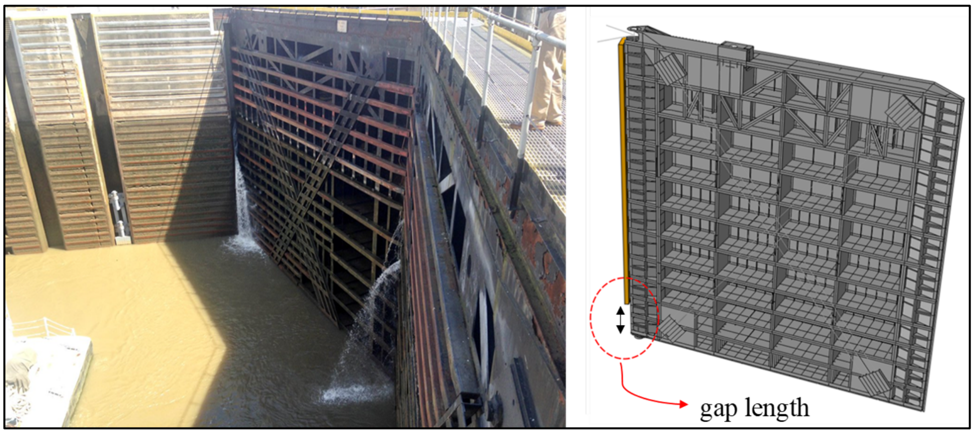

Figure 11: Miter Gate and physical-based FE model

In the next section, the generated data from multiple (i.e. 46 sensors) strain gauges will be used to develop diagnostics and prognostics capabilities for bearing gaps in miter gates.

6.2 Sequential damage detection using physics-based simulation

As discussed earlier, if continuous monitoring is introduced with the Markov transition matrix then the optimal maintenance plan over time can be updated based on the information gained by the sensor information using sequential damage estimation.

As discussed in Sec. 5.1, the likelihood function $f(\mathbf{s}_n \mid a_n)$ needs to be evaluated numerous times during the sequential damage estimation, which is computationally expensive especially because of the number of DOF in a FE model of a miter gate. A surrogate model is constructed to map the relation from gap length (and other model parameters such as hydrostatic and thermal loads applied to miter gates) to the strain response at the strain gauges locations as shown in Figure 12. This figure shows the locations where the strain information is extracted from the physical based model to train the Kriging surrogate model. The sensor location matches with SHM strain network installed at the Greenup miter gate.

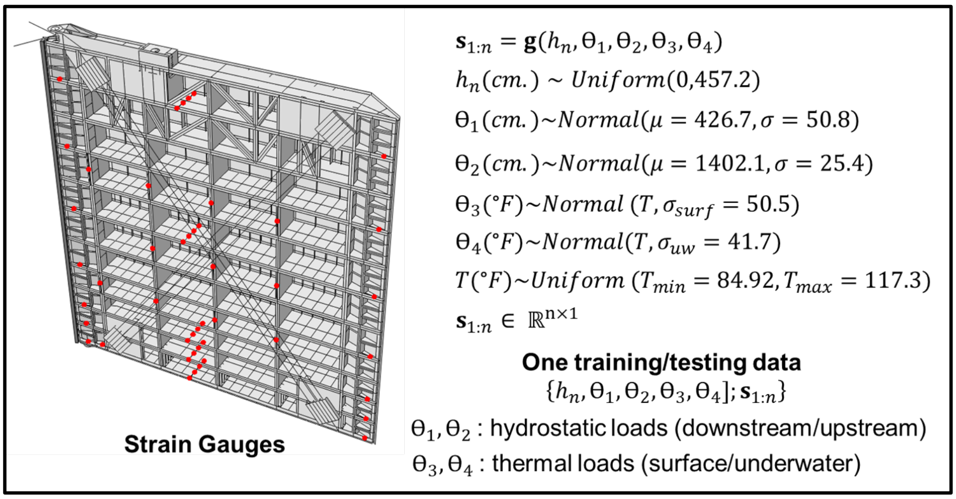

Figure 12: Sensor locations, and data generated to train surrogate model

Figure 13 shows the Kriging model testing accuracy at one strain SVD important feature (left) for different input values (i.e. gap length and other model inputs such as hydrostatic and thermal loads applied to miter gates) and the strain accuracy (in the original strain space) at different strain gauges locations for the same input value.

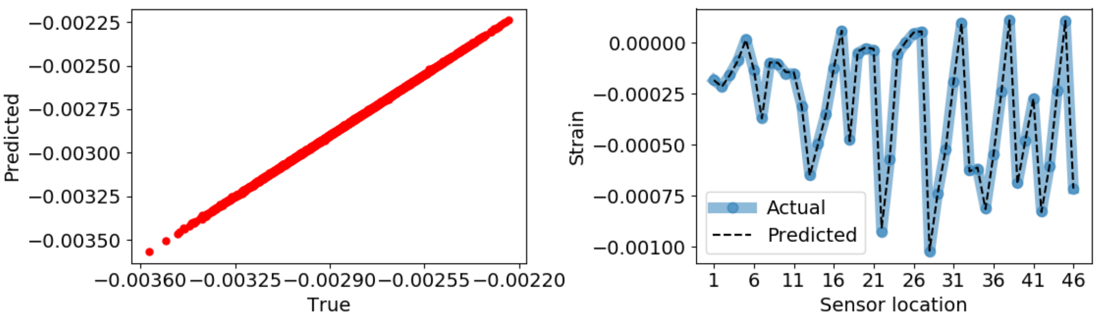

Figure 13: Surrogate modelling accuracy validation

Synthetic input parameters are generated using an autoregressive–moving-average (ARMA) model. These inputs are evaluated with the validated kriging model to generate strain time series measurements at every strain gauge location of the miter gate as shown in Figure 14.

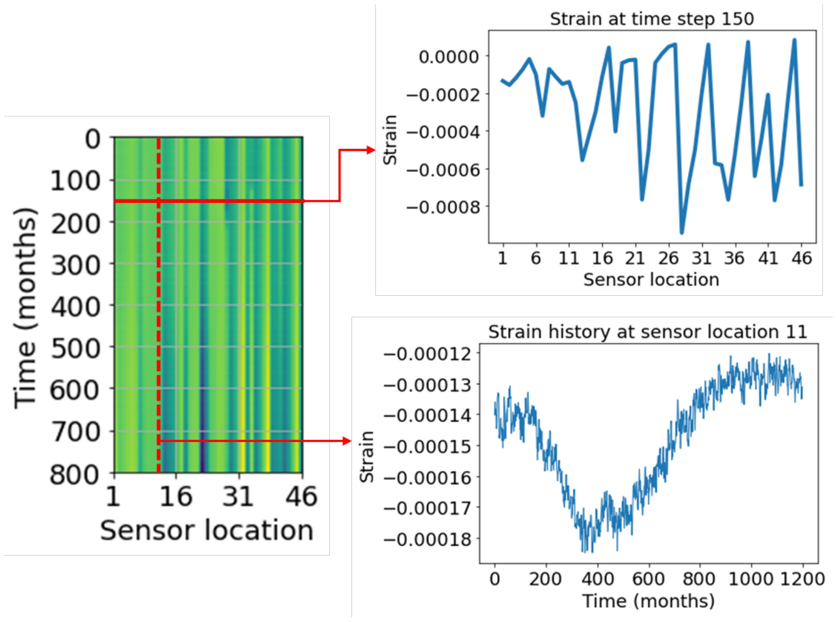

Figure 14: Strain observations from sensors

Following the method discussed in Sec. 5.1, the posterior $f(h_n \mid \mathbf{s}_{1:n})$ distribution of the gap length may be updated dynamically as strain measurements are available from the SHM network system. Figure 15 shows the updated predictions of the gap length against the true damage.

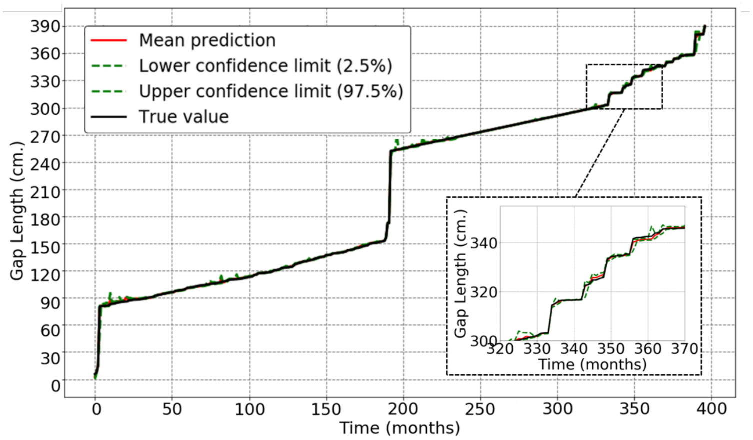

Figure 15: Damage detection over time using the state equation given in Eq. (22)

The result in Figure 15 shows that the proposed sequential damage estimation method is able to accurately estimate the damaged gap length based on the strain measurement data from the 46 sensors as indicated in Figure 12.

6.3 Estimation of "B" ratings error ratio based on online damage estimation

As described in Sec. 5.2 and indicated in Figure 10, the variable, $\gamma = B_{\text{inspected}} / B_{\text{total}}$, can be recursively updated using the observations obtained from the physics-based damage estimation. To achieve this, firstly, a mapping between gap length to the OCA condition rating is needing following Eq. (29). In this application, a uniform mapping consisting on gap length increments of 30 in. (76.2 cm.) was used as shown in Table 2.

Table 2: State mapping from discrete to continuous

OCA rating	Gap length (cm)
IA	$0 \le h_n < 76.2$
IB	$76.2 \le h_n < 152.4$
IC	$152.4 \le h_n < 228.6$
ID	$228.6 \le h_n < 304.8$
IF	$304.8 \le h_n < 381$
ICF	$h_n > 381$

Following that, the "B" rating error ratio is updated based on the damage estimation. Figure 16 shows the mean prediction and the 95% confidence intervals obtained for γ. As the information is acquired from the physics-based diagnosis, the variance of γ reduces significantly. Also, it is noted that as the quoin block has already surpassed the B condition, the value of γ approaches the true value (an assumed ground truth value in Sec. 6.2 that is used to generated the synthetic strain measurement data based on a gap growth model). This demonstrates the effectiveness of the proposed Bayesian updating scheme in estimating the "B" ratings error ratio. It worth mentioning that the error ratio updating is mainly affected by the gap length profile as given in Figure 15. The gap length profile is just one realization of the underlying degradation model. Since it is just one realization of many possible gap growth profiles, it leads to a small bias between the estimated error ratio and the "true" error ratio used in Sec. 6.2.

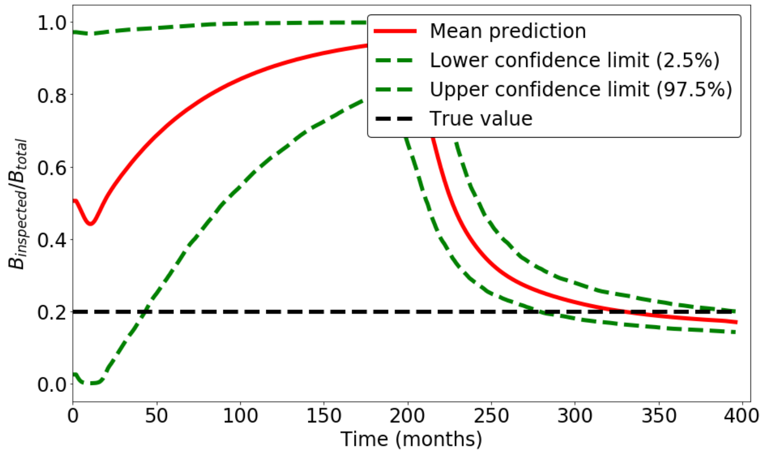

Figure 16: "B" ratings error ratio (γ) estimation

6.4 Failure prognosis and optimal maintenance planning for the miter gate

To demonstrate the improvement on the gap length prognosis, the updated over time RUL can be evaluated, and compared against its true value. Figure 17 shows that the RUL estimation using the state equation given in Eq. (22). It shows that the random-walk state equation could lead to large errors in RUL estimate even if it can effectively perform damage detection. As been discussed in Sec. 5.3, the information from the OCA rating can be used to improve the prognosis capabilities and overcome the limitations of the state equation in Eq. (22). Figure 18 shows that the proposed hybrid prognosis method can improve the accuracy RUL estimation while effectively performing damage detection. The jumps in Figure 18 are attributed to the discrete nature of the OCA ratings.

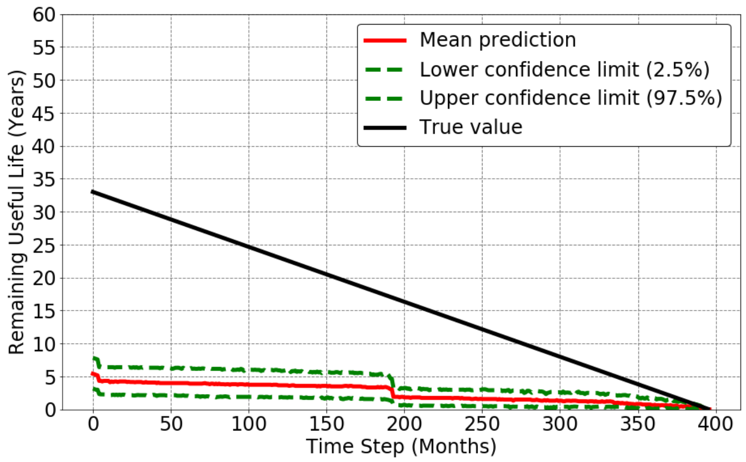

Figure 17: RUL estimate using the state equation given in Eq. (22)

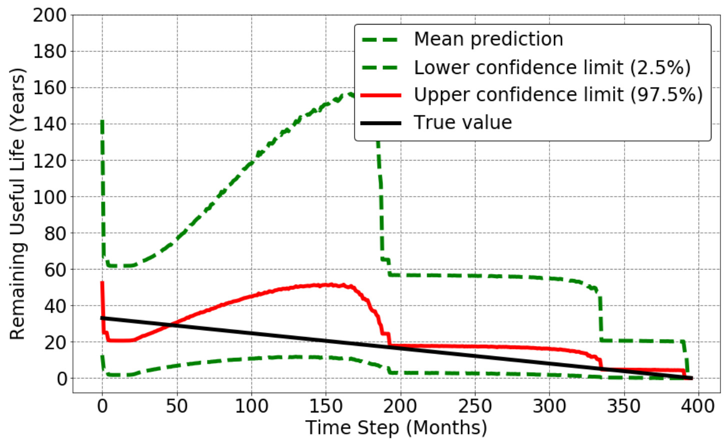

Figure 18: RUL estimate using the proposed method

Figure 19 and 20 show how the minimum CPUT and the optimal maintenance time are updated from the strain measurements over time. These figures were generated using a uniform mapping between the gap length to the OCA ratings as given in Table 2. The vertical line in these figures represent the true end of life. In other words, the true end of life is when the gap length reaches the value of 150 inch (381 cm.), which corresponds to the "CF" condition. As noted, the minimum CPUT mainly increase with time, indicating that the denominator in Eq. (43) is approaching to zero as the term $F_{t|\mathbf{s}_{1:n}}(\tau)$ is approaching to 1. Similarly, in contrast to the static maintenance planning in Sec. 4, the optimal maintenance time (relative to the current time) can be updated dynamically as time passes based on the information collected from the SHM system.

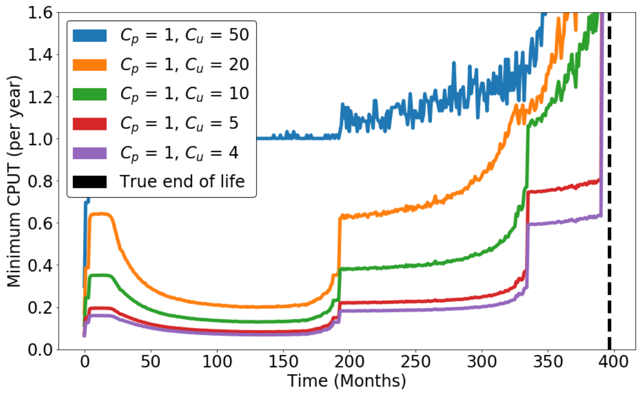

Figure 19: Minimum CPUT corresponding to different values of Cp and Cu

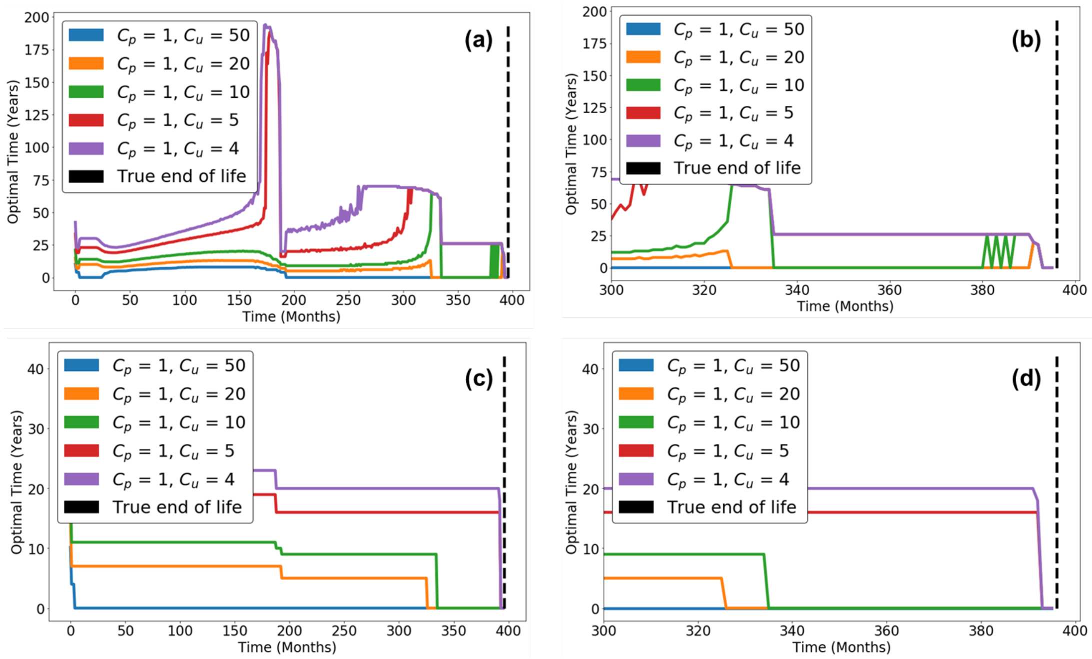

Figure 20: a) Optimal maintenance time corresponding to different Cp and Cu, b) optimal maintenance time approaching end of life, c) alternative optimal maintenance time corresponding to different Cp and Cu , and d) alternative optimal maintenance time approaching end of life

One of the main reasons why the optimal time (see Figure 20a), especially for low cost ratios, increases so dramatically at around 175 month is due to the nature of Eq. (43) and (12). In these cases, the CPUT curve obtained from Eq. (43) tends to be very flat. In other words, many different maintenance times may have basically the same CPUT value. For Figure 20c, a conservative selection for the optimal maintenance is carried out, and it is assumed that the updated optimal maintenance tends to decrease with time and holds practically the same CPUT value. Thus, with this conservative selection, the minimum

CPUT corresponding to different values of Cp and Cu would show basically the same results as Figure 19.

7. Conclusions

A Markov process is used to approximate the unreliability function using inspection ratings from quoin block in miter gates. A cost function, that weight the preventive and emergency costs associated for the rehabilitation of a structural component, is used to come up with the optimal maintenance time. It is shown that the uncertainties in the transition matrix derived from visual inspections affects the optimal maintenance time. To reduce the uncertainty in the optimal maintenance time, a framework is introduced to combine continuous structural health monitoring with the Markov transition matrix. This approach allows to update the optimal maintenance plan as well as the error ratio of the OCA ratings over time based on the information gained by the sensor information using sequential damage estimation. This approach can be applicable to different nonrepairable components in miter gates, which may have different transition matrices values. However, further work needs to be done to extend this methodology to other components in miter gates and then from miter gate components to whole miter gate system level (e.g. including all critical miter gate components).

Acknowledgements: Funding for this work was provided by the United States Army Corps of Engineers through the U.S. Army Engineer Research and Development Center Research Cooperative Agreement W912HZ-17-2-0024.

References

[1] U.S. Army Corps of Engineers Headquarters. Navigation 2018. http://www.usace.army.mil/Missions/CivilWorks/Navigation.aspx (accessed August 1, 2018).

[2] Foltz SD. Investigation of Mechanical Breakdowns Leading to Lock Closures. Champaign, IL: 2017.

[3] U.S. Army Corps of Engineers Headquarters. SMART GATE 2007. https://www.erdc.usace.army.mil/Media/Fact-Sheets/Fact-Sheet-Article-View/Article/476668/smart-gate/ (accessed August 1, 2018).

[4] Daniel R, Paulus T. Hydraulic Gates in View of Asset Management. Lock Gates Other Closures Hydraul. Proj., Elsevier; 2019, p. 945–60. https://doi.org/10.1016/B978-0-12-809264-4.00017-3.

[5] Eick BA, Treece ZR, Spencer BF, Smith MD, Sweeney SC, Alexander QG, et al. Automated damage detection in miter gates of navigation locks. Struct Control Heal Monit 2018;25:1–18. https://doi.org/10.1002/stc.2053.

[6] Vega MA, Todd MD. A variational Bayesian neural network for structural health monitoring and cost-informed decision-making in miter gates. Struct Heal Monit 2020. https://doi.org/10.1177/1475921720904543.

[7] Eick BA, Smith MD, Fillmore TB. Feasibility of retrofitting existing miter-type lock gates with discontinuous contact blocks. J Struct Integr Maint 2019;4:179–94. https://doi.org/10.1080/24705314.2019.1657617.

[8] Yam RCM, Tse PW, Li L, Tu P. Intelligent Predictive Decision Support System for Condition-Based Maintenance. Int J Adv Manuf Technol 2001;17:383–91. https://doi.org/10.1007/s001700170173.

[9] Weibull W. A Statistical Distribution Function of Wide Applicability. J Appl Mech 1951;103:293–7.

[10] Barlow R, Hunter L. Optimum Preventive Maintenance Policies. Oper Res 1960;8:90–100. https://doi.org/10.1287/opre.8.1.90.

[11] Das AN, Acharya D. Age Replacement of Components During IFR Delay Time. IEEE Trans Reliab 2004;53:306–12. https://doi.org/10.1109/TR.2004.833422.

[12] Castro IT, Sule Alfa A. Lifetime replacement policy in discrete time for a single unit system. Reliab Eng Syst Saf 2004;84:103–11. https://doi.org/10.1016/j.ress.2003.11.005.

[13] Nakagawa T, Yasui K. Note on optimal redundant policies for reliability models. J Qual Maint Eng 2005;11:82–96. https://doi.org/10.1108/13552510510589398.

[14] Childress S, Durango-Cohen P. On parallel machine replacement problems with general replacement cost functions and stochastic deterioration. Nav Res Logist 2005;52:409–19. https://doi.org/10.1002/nav.20088.

[15] Ahmad R, Kamaruddin S. An overview of time-based and condition-based maintenance in industrial application. Comput Ind Eng 2012;63:135–49. https://doi.org/10.1016/j.cie.2012.02.002.

[16] Zhu Y, Elsayed EA, Liao H, Chan LY. Availability optimization of systems subject to

competing risk. Eur J Oper Res 2010;202:781–8. https://doi.org/10.1016/j.ejor.2009.06.008.

[17] Tian Z, Jin T, Wu B, Ding F. Condition based maintenance optimization for wind power generation systems under continuous monitoring. Renew Energy 2011;36:1502–9. https://doi.org/10.1016/j.renene.2010.10.028.

[18] Tian Z, Liao H. Condition based maintenance optimization for multi-component systems using proportional hazards model. Reliab Eng Syst Saf 2011;96:581–9. https://doi.org/10.1016/j.ress.2010.12.023.

[19] Alaswad S, Xiang Y. A review on condition-based maintenance optimization models for stochastically deteriorating system. Reliab Eng Syst Saf 2017;157:54–63. https://doi.org/10.1016/j.ress.2016.08.009.

[20] Petcherdchoo A, Neves LA, Frangopol DM. Optimizing Lifetime Condition and Reliability of Deteriorating Structures with Emphasis on Bridges. J Struct Eng 2008;134:544–52. https://doi.org/10.1061/(ASCE)0733-9445(2008)134:4(544).

[21] Saydam D, Frangopol DM. Risk-Based Maintenance Optimization of Deteriorating Bridges. J Struct Eng 2015;141:04014120. https://doi.org/10.1061/(ASCE)ST.1943-541X.0001038.

[22] Gong C, Frangopol DM. Condition-Based Multiobjective Maintenance Decision Making for Highway Bridges Considering Risk Perceptions. J Struct Eng 2020;146:04020051. https://doi.org/10.1061/(ASCE)ST.1943-541X.0002570.

[23] Orchard ME, Vachtsevanos GJ. A Particle Filtering Approach for On-Line Failure Prognosis in a Planetary Carrier Plate. Int J Fuzzy Log Intell Syst 2007;7:221–7. https://doi.org/10.5391/IJFIS.2007.7.4.221.

[24] Daigle M, Goebel K. Multiple damage progression paths in model-based prognostics. 2011 Aerosp. Conf., IEEE; 2011, p. 1–10. https://doi.org/10.1109/AERO.2011.5747574.

[25] An D, Choi J-H, Schmitz TL, Kim NH. In situ monitoring and prediction of progressive joint wear using Bayesian statistics. Wear 2011;270:828–38. https://doi.org/10.1016/j.wear.2011.02.010.

[26] Zio E, Di Maio F. A data-driven fuzzy approach for predicting the remaining useful life in dynamic failure scenarios of a nuclear system. Reliab Eng Syst Saf 2010;95:49–57. https://doi.org/10.1016/j.ress.2009.08.001.

[27] Mohanty S, Das S, Chattopadhyay A, Peralta P. Gaussian Process Time Series Model for Life Prognosis of Metallic Structures. J Intell Mater Syst Struct 2009;20:887–96. https://doi.org/10.1177/1045389X08099602.

[28] Galar D, Kumar U, Lee J, Zhao W. Remaining Useful Life Estimation using Time Trajectory Tracking and Support Vector Machines. J Phys Conf Ser 2012;364:012063. https://doi.org/10.1088/1742-6596/364/1/012063.

[29] Ye Z-S, Xie M. Stochastic modelling and analysis of degradation for highly reliable products. Appl Stoch Model Bus Ind 2015;31:16–32. https://doi.org/10.1002/asmb.2063.

[30] Xu J, Xu L. Health management based on fusion prognostics for avionics systems. J Syst Eng Electron 2011;22:428–36. https://doi.org/10.3969/j.issn.1004-4132.2011.03.010.

[31] Liao L, Kottig F. Review of Hybrid Prognostics Approaches for Remaining Useful Life Prediction of Engineered Systems, and an Application to Battery Life Prediction. IEEE Trans Reliab 2014;63:191–207. https://doi.org/10.1109/TR.2014.2299152.

[32] Przybyla J. Best Practices in Asset Management. Alexandria, Virginia: 2013.

[33] An D, Kim NH, Choi J-H. Practical options for selecting data-driven or physics-based prognostics algorithms with reviews. Reliab Eng Syst Saf 2015;133:223–36. https://doi.org/10.1016/j.ress.2014.09.014.

[34] Vega MA, Madarshahian R, Fillmore TB, Todd MD. Optimal Maintenance Decision for Deteriorating Components in Miter Gates Using Markov Chain Prediction Model. Struct. Heal. Monit. 2019 Enabling Intell. Life-cycle Heal. Manag. Ind. Internet Things, Lancaster, PA: DEStech Publications, Inc.; 2019, p. 1471–8. https://doi.org/10.12783/shm2019/32269.

[35] Jiang R, Murthy DNP. A study of Weibull shape parameter: Properties and significance. Reliab Eng Syst Saf 2011;96:1619–26. https://doi.org/10.1016/j.ress.2011.09.003.

[36] USACE. Policy for Operational Condition Assessments of USACE Assets 2019:13. https://www.publications.usace.army.mil/Portals/76/Users/182/86/2486/EC-11-2-218.pdf?ver=2019-09-04-162858-440.

[37] Orchard M, Kacprzynski G, Goebel K, Saha B, Vachtsevanos G. Advances in uncertainty representation and management for particle filtering applied to prognostics. 2008 Int. Conf. Progn. Heal. Manag., IEEE; 2008, p. 1–6. https://doi.org/10.1109/PHM.2008.4711433.

[38] Daniel R, Paulus T. Detailed Gate Design☆. Lock Gates Other Closures Hydraul. Proj., Elsevier; 2019, p. 531–620. https://doi.org/10.1016/B978-0-12-809264-4.00008-2.